Antiferroelectric Phase Evolution in $Hf_xZr_{1-x}O_2$ Thin Film Toward High Endurance of Non-Volatile Memory Devices

Danyang Chen, Shuman Zhong, Yulong Dong, Tianning Cui, Jingquan Liu, *Member, IEEE*, Mengwei Si, *Member, IEEE*, and Xiuyan Li

***Abstract*— In this study, we experimentally and theoretically demonstrated a universal pathway of hysteresis evolution in polarization switching cycling in both antiferroelectric (AFE) and ferroelectric (FE) $Hf_xZr_{1-x}O_2$ (HZO) thin films. AFE films can achieve sufficient remnant polarization and high endurance by engineering the evolution process of double hysteresis merge. Based on this, we propose a new strategy for realizing high-endurance AFE films in non-volatile memory devices. Additionally, a record high endurance $>10^{12}$ on 6 nm AFE HZO under full polarization switching conditions at 4.5 MV/cm and 1 MHz is achieved to demonstrate the potential of this strategy.**

***Index Terms*— Antiferroelectric materials, sub-loop, remnant polarization, coercive field, endurance, hafnium zirconium oxide.**

I. Introduction

HfO_2-BASED ferroelectrics (FE) have attracted considerable attention since their discovery in 2011 because of their complementary metal oxide semiconductor (CMOS) compatibility, high scalability, and environmentally friendly composition. These advantage enable them to overcome critical obstacles in the application of conventional ferroelectric material in non-volatile memory (NVM) devices [1], [2]. One of the primary concerns for memory devices is endurance performance, which determines device reliability in practical applications. However, HfO_2-based FE materials show strong wake-up and fatigue effects in polarization cycling, significantly degrading the endurance performance [3], [4], [5], [6], [7], [8], [9], [10], [11], [12], [13], [14], [15], [16], [17].

Over a decade, intensive studies have focused on enhancing the endurance of memory devices. Several strategies have been proposed, including engineering of rapid thermal annealing (RTA) [3], [4], film deposition process [5], [6], film thickness [7], interface [8], [9] and electrodes [10], [11]. In some cases, it was found that an AFE-like characteristics appeared pristinely and it waked up to FE one for FE-HZO films.

On the other hand, AFE-$Hf_xZr_{1-x}O_2$ (HZO) thin films with higher Zr concentration exhibit higher endurance with respect to their FE counterparts. This is considered to be benefit from uniform phase distribution and an insignificant increase in the leakage current during cycling in the AFE case [18], [19]. Generally, AFE films are not suitable for non-volatile storage because they have no remnant polarization at zero voltage. Recently, a couple of approaches to tuning the material properties have been proposed to materialize its high-endurance strength in NVM, such as using its sub-loop by engineering a built-in field or making an AFE/FE bilayer [12], [20], [21], [22], [23].

In this study, we found a universal transition from AFE to FE characteristics numerically and theoretically during polarization switching cycling in both typical AFE and FE $Hf_xZr_{1-x}O_2$ films. This correlates with the special wake-up effect in FE films with the AFE system. Based on this, a new approach is proposed to materialize the high endurance of AFE films by engineering the transition process. This approach achieves sufficient P_r and high-field operations. Furthermore, we demonstrate high endurance of $>10^{12}$ under 4.5 MV/cm with $2P_r > 15\ \mu C/cm^2$ on a 6 nm $Hf_{0.2}Zr_{0.8}O_2$ thin film, which is a record high number in HZO systems, considering the full polarization switching conditions. Our results provide a guideline for the high endurance of FE-NVM design, particularly for the application of AFE film in the NVM system.

II. Experimental

Typical AFE and FE $Hf_xZr_{1-x}O_2$ metal-ferroelectric-metal (MFM) capacitors with $x = 0$, 0.2, or 0.5, were fabricated and characterized. The key process flow is shown in Fig. 1(a). After RCA cleaning, 30 nm TiN films were deposited by reactive magnetron sputtering on a highly doped Si wafer followed by 6 or 15 nm $Hf_xZr_{1-x}O_2$ film deposition by atomic layer deposition (ALD) at 250°C. The precursors and oxidant were TEMAHf, TEMAZr, and H_2O. Then, 30 nm TiN and 30 nm W were deposited by sputtering as top electrodes and patterned using photo-lithography and a lift-off process. Finally, the HZO capacitors were post-metallization annealed (PMA) at 550°C in N_2 ambient for 30 s.

The cross-sectional transmission electron microscope (TEM) images of typical FE and AFE capacitors with 6 nm $Hf_xZr_{1-x}O_2$ films are shown in Fig. 1(b). Additionally, the crystalline structure of the $Hf_xZr_{1-x}O_2$ films was characterized

Manuscript received 3 October 2022; revised 22 October 2022; accepted 25 October 2022. Date of publication 31 October 2022; date of current version 28 November 2022. This work was supported by the National Natural Science Foundation of China under Grant 91964110, Grant 61904103, and Grant 62111540163. The review of this letter was arranged by Editor S. Yu. *(Corresponding author: Xiuyan Li.)*

Danyang Chen, Shuman Zhong, Yulong Dong, and Tianning Cui are with the National Key Laboratory of Science and Technology on Micro/Nano Fabrication, Shanghai Jiao Tong University, Shanghai 200240, China, and also with the Department of Micro/Nano Electronics, School of Electronic Information and Electrical Engineering, Shanghai Jiao Tong university, Shanghai 200240, China.

Jingquan Liu and Xiuyan Li are with the National Key Laboratory of Science and Technology on Micro/Nano Fabrication, Shanghai Jiao Tong University, Shanghai 200240, China (e-mail: xiuyanli@sjtu.edu.cn).

Mengwei Si is with the Department of Electronic Engineering, Shanghai Jiao Tong University, Shanghai 200240, China.

Color versions of one or more figures in this letter are available at https://doi.org/10.1109/LED.2022.3217813.

Digital Object Identifier 10.1109/LED.2022.3217813

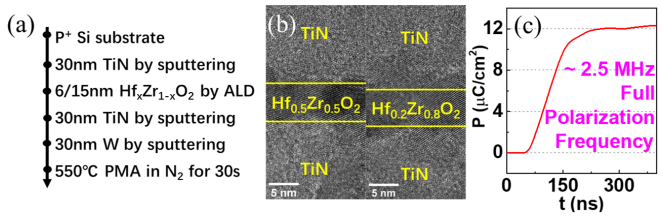

Fig. 1. (a) Process flow of $Hf_xZr_{1-x}O_2$ MFM capacitors with x = 0, 0.2, 0.5. (b) TEM images of typical FE and AFE capacitors with 6 nm $Hf_xZr_{1-x}O_2$. (c) Switching time of 6 nm $Hf_{0.2}Zr_{0.8}O_2$ film after 10^9 cycles wake-up.

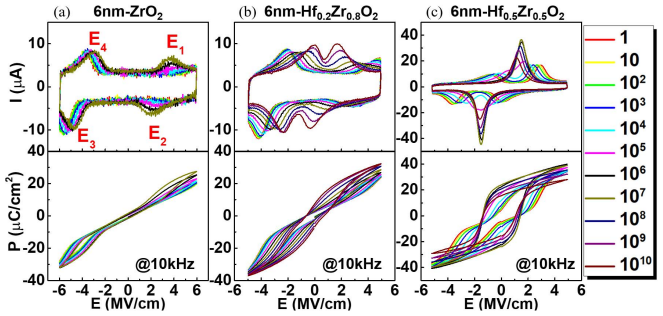

Fig. 2. I-E and P-E loops of 6 nm (a) ZrO_2 (b) $Hf_{0.2}Zr_{0.8}O_2$ (c) $Hf_{0.5}Zr_{0.5}O_2$ films during cycling.

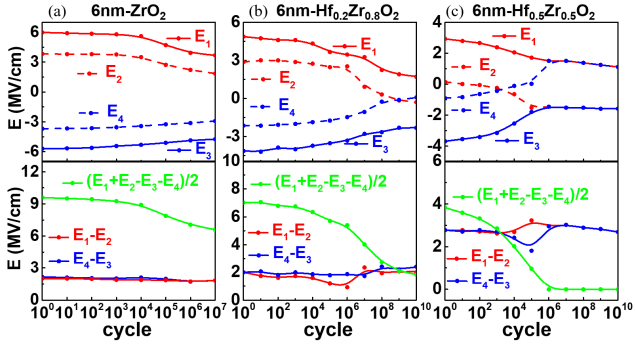

Fig. 3. Coercive fields of 6 nm (a) ZrO_2 (b) $Hf_{0.2}Zr_{0.8}O_2$ (c) $Hf_{0.5}Zr_{0.5}O_2$ films during cycling.

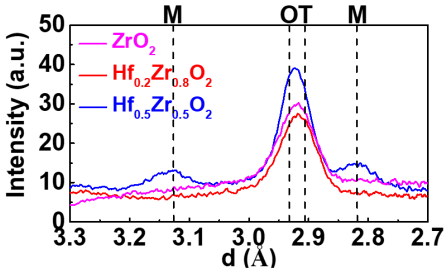

Fig. 4. GIXRD results of 6 nm $Hf_xZr_{1-x}O_2$ films (x = 0, 0.2, 0.5).

using synchrotron-based grazing incidence X-ray diffraction (GIXRD) at 10 keV. Keithley 4200A-SCS was used to perform the electrical tests. Polarization-field (P-E) and current-field (I-E) tests were performed at 10 kHz while endurance tests were performed at 1 MHz with a field of 4.5 MV/cm. Note that the conditions of the endurance tests ensure full polarization switching as shown in Fig. 1(c).

III. Results and Discussion

Fig. 2 shows I-E and P-E loops measured on 6 nm AFE ZrO_2, $Hf_{0.2}Zr_{0.8}O_2$ and FE $Hf_{0.5}Zr_{0.5}O_2$ films. AFE-like to FE (AFE-FE) evolution as a wake-up effect is observed in 10^6 polarization switching cycling for the FE $Hf_{0.5}Zr_{0.5}O_2$ device, as reported in the literature. Although AFE characteristics are maintained in $Hf_{0.2}Zr_{0.8}O_2$ films at the end of the cycling, the positions of two sub-loops are closed with each other, and P_r increases during the cycling. A similar merging of two sub-loops was observed in the ZrO_2 film. We also observed a similar trend in 15 nm films with three types of Zr contents (not shown). These results indicate that a similar evolution in polarization switching cycling occurs in both typical FE and AFE films. Note that the P_r in ZrO_2 film remains unchanged and a relatively high operation field (6 MV/cm) is required for the ZrO_2 device, indicating that it become difficult to obtain AFE-FE evolution with higher Zr content.

To obtain a quantitative analysis of the evolution process in AFE and FE films, the coercive fields of each sub–loop, E_1/E_2 for positive and E_3/E_4 for negative, marked in Fig. 2(a), are extracted and plotted as a function of cycles in Fig. 3. The coercive fields of each sub-loop approach to that of another are indicated by the change in $(E_1+E_2-E_3-E_4)/2$. Interestingly, the relative position of the coercive field for each sub-loop (values of E_1-E_2 and E_3-E_4) remains almost unchanged.

It is well-known that AFE film is mainly with tetragonal (T) phase while polarization properties in FE films is associated with orthorhombic (O) phase for $Hf_xZr_{1-x}O_2$ material [23]. And a reversible T-O phase transition in an electric field has been proposed as the origin of the AFE characteristics [24]. We also performed GIXRD characterization on the films with three types of Zr concentrations discussed above. The results in Fig. 4 show that monoclinic (M) phases are mixed with T/O phases in 6 nm $Hf_{0.5}Zr_{0.5}O_2$ film, whereas ZrO_2 and $Hf_{0.2}Zr_{0.8}O_2$ films may be mainly with the T phase in the pristine state. The results are consistent with those reported.

Based on the above analysis, an energetic analysis was performed using the Landau-Ginzburg-Devonshire (LGD) equation as follows:

$$G(P) = \frac{\alpha}{2}P^2 + \frac{\beta}{4}P^4 + \frac{\gamma}{6}P^6 - EP \quad (1)$$

where α, β, γ are Landau expansion coefficients [21], [25]. We assume that the AFE characteristics are due to a reversible T-O transition, which is case for first-order phase transitions [24]. Namely, $\beta < 0$ and $\gamma > 0$ [26]. Therefore, the P-E loops are derived from G'(P) = 0. Additionally, switching fields are derived from G'(P) = 0 and G"(P) = 0.

Fig. 5 shows the generated G-P and P-E curves by varying α with fixed β and γ. When $0 \le \alpha < 9\beta^2/20\gamma$, G'(P) = 0 and G"(P) = 0 have four real solutions and three energy wells. In this case, typical AFE characteristics are obtained and we assume three energy wells are corresponding to the O↑, T and O↓ phases, respectively, as shown in Figs. 5(a)-(f). Accordingly, there are four switching fields ($E_1/E_2/E_3/E_4$) and two sub-loops in P-E curve. With α decreasing, the energy of three potential wells changes relatively. Namely, the energy of O phase lowers relative to that of T phase. Correspondingly, two sub-loops in P-E characteristics close to each other. This is similar to the results shown in Fig. 2. Besides, there is a special case as shown in Figs. 5(e) and (f), where an AFE-like shape in the energy curve and an FE-like shape in the P-E characteristics exist simultaneously. Here, the T-O↓ phase transition (E_1) may occur immediately after the O↑-T transition (E_4) because $E_4 \ge E_1$, indicating that,

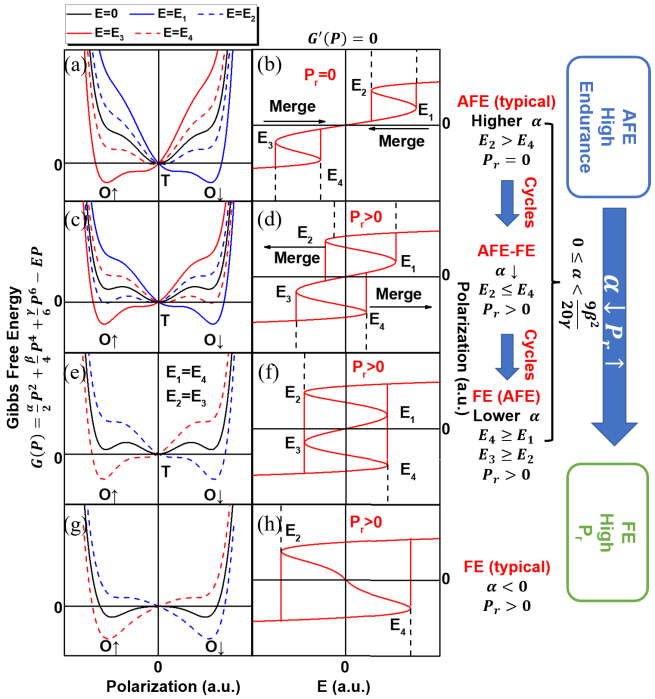

Fig. 5. Gibbs free energy (G(P)) and P-E loops extracted from G'(P) = 0 of (a)(b) AFE, (c)(d) AFE-FE, (e)(f) FE (AFE) and (g)(h) typical FE materials with/without external field (E).

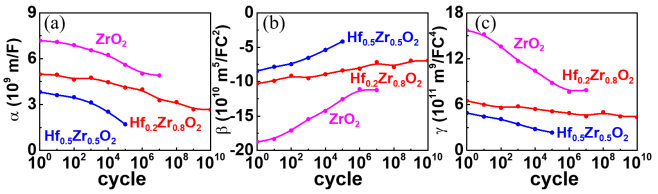

Fig. 6. Landau expansion coefficients of 6 nm ZrO_2, $Hf_{0.5}Zr_{0.5}O_2$ and $Hf_{0.2}Zr_{0.8}O_2$ films during cycling. (a) α, (b) β, (c) γ.

interestingly, FE hysteresis can be explained not only by negative α, as shown in Figs. 5(g) and (h).

Note that only a decrease in α leads to an increase in E_1-E_2 as shown in Fig. 5, which is inconsistent with the almost unchanged E_1-E_2 as shown in Fig. 3. Several studies have reported that material changes can affect three Landau coefficients simultaneously [27], [28]. Therefore, we suspect that β and γ are also changed during cycling.

To more intuitively understand this, α, β, γ were extracted by substituting the experimental value of $E_1/E_2/E_3/E_4$ into $G'(P) = 0$, $G''(P) = 0$ and assuming $G'(P_s) = 0$, where P_s is the saturation polarization. The results in Fig. 6(a) show that α decreases during cycling, which is consistent with the above theoretical analysis. Furthermore, $|\beta|$ and γ decrease during cycling. Glinchuk reported that the Landau coefficients were related to the average concentration of oxygen vacancies [28]. Additionally, Schenk proposed that the merge-like wake-up process in HfO_2-based FE film due to the redistribution of charged defects, such as oxygen vacancies [29]. We considered that the change in the Landau expansion coefficients and constant E_1-E_2/E_3-E_4 may be due to the redistribution of charged defects, such as oxygen vacancies.

Concerning application of aforementioned AFE/FE films in NVM devices, both high endurance and sufficient remnant

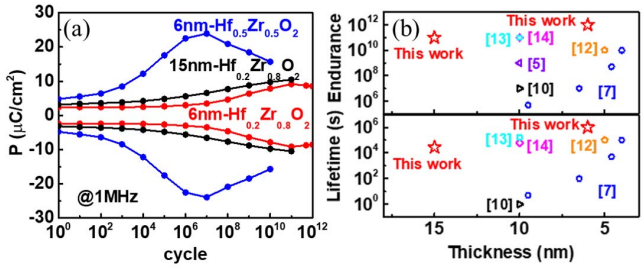

Fig. 7. (a) Endurance characteristics of $Hf_{0.5}Zr_{0.5}O_2$ and $Hf_{0.2}Zr_{0.8}O_2$ films. (b) Benchmark of HZO in terms of endurance and effective lifetime.

polarization ($2P_r > 10$ $\mu C/cm^2$) are required. Thus, it is possible to use the high-endurance strength of AFE by engineering the evolution process to obtain sufficient P_r in conjunction with maintaining basic AFE characteristics. Namely, a new method for combining the advantages of high P_r of FE and high endurance of AFE is achievable. Either early breakdown due to too high operation field, as in the ZrO_2 case, or full transition to FE characteristics, as in the $Hf_{0.5}Zr_{0.5}O_2$ case, can degrade endurance performance, so both should be suppressed.

To verify this strategy, the endurance performance of the aforementioned films was characterized at 4.5 MV/cm and 1 MHz, as shown in Fig. 7(a). Compared to the 10^{10} endurance performance of a typical 6 nm FE film, 10^{11} and 10^{12} cycles are achieved using 15 and 6 nm AFE films, respectively. Additionally, $2P_r > 10$ $\mu C/cm^2$ is achieved after 10^8 cycles. Because no breakdown and obvious fatigue are observed for the 6 nm AFE film even after 10^{12} cycles, its intrinsic endurance should be higher. This result demonstrates the proposed method's potential for increasing endurance. Note that the breakdown performance of AFE devices is also better than that of FE, and it is even better for thinner AFE films. The FE film breakdown has been reported to be related to M phase generation [15]. And it is well known that M phase formation in pristine films is suppressed by decreasing film thickness or increasing the doping concentration. Therefore, it is understandable that the AFE film with a suitable concentration of T phase will not only slow-down the evolution process but also delay the film breakdown.

In addition, $>10^{12}$ endurance and corresponding $>10^6$ s effective lifetime are record high values considering the full switching conditions with relatively high field and low frequency, as compared in Fig. 7(b). The endurance of HZO could be much more over-estimated under high frequencies or low electrical fields because polarization is switched partially.

IV. Conclusion

In conclusion, a universal evolution from AFE to FE characteristics in both typical AFE and FE HZO film composition has been confirmed by experimental and theoretical analysis of the change in hysteresis loops. The evolution could be due to the change in relative energy between the T and O phases caused by repeated electric field cycling. High endurance with sufficient P_r can be achieved by controlling the evolution process of AFE film. Based this, a new method for incorporating AFE film in NVM is proposed and a record high endurance $>10^{12}$ on 6-nm-thick $Hf_{0.2}Zr_{0.8}O_2$ with full polarization switching under high field was demonstrated.

REFERENCES

[1] T. S. Böscke, J. Müller, D. Bräuhaus, U. Schröder, and U. Böttger, "Ferroelectricity in hafnium oxide: CMOS compatible ferroelectric field effect transistors," *IEDM Tech. Dig.*, Dec. 2011, pp. 24.5.1–24.5.4, doi: 10.1109/IEDM.2011.6131606.

[2] J. Müller, T. S. Böscke, U. Schröder, S. Mueller, D. Bräuhaus, U. Böttger, L. Frey, and T. Mikolajick, "Ferroelectricity in simple binary ZrO_2 and HfO_2," *Nano Lett.*, vol. 12, no. 8, pp. 4318–4323, Aug. 2012, doi: 10.1021/nl302049k.

[3] W. Wei, W. Zhang, F. Wang, X. Ma, Q. Wang, P. Sang, X. Zhan, Y. Li, L. Tai, Q. Luo, H. Lv, and J. Chen, "Deep insights into the failure mechanisms in field-cycled ferroelectric $Hf_{0.5}Zr_{0.5}O_2$ thin film: TDDB characterizations and first-principles calculations," *IEDM Tech. Dig.*, Dec. 2020, pp. 39.6.1–39.6.4, doi: 10.1109/IEDM13553.2020.9371932.

[4] T. Mittmann, F. P. G. Fengler, C. Richter, M. H. Park, T. Mikolajick, and U. Schroeder, "Optimizing process conditions for improved $Hf_{1-x}ZrxO_2$ ferroelectric capacitor performance," *Microelectronic Eng.*, vol. 178, pp. 48–51, Jun. 2017, doi: 10.1016/j.mee.2017.04.031.

[5] T. Mittmann, M. Materano, S.-C. Chang, I. Karpov, T. Mikolajick, and U. Schroeder, "Impact of oxygen vacancy content in ferroelectric HZO films on the device performance," in *IEDM Tech. Dig.*, Dec. 2020, p. 18, doi: 10.1109/IEDM13553.2020.9372097.

[6] A. G. Chernikova, M. G. Kozodaev, R. R. Khakimov, S. N. Polyakov, and A. M. Markeev, "Influence of ALD Ru bottom electrode on ferroelectric properties of $Hf_{0.5}Zr_{0.5}O_2$-based capacitors," *Appl. Phys. Lett.*, vol. 117, no. 19, Nov. 2020, Art. no. 192902, doi: 10.1063/5.0022118.

[7] K. Tahara, K. Toprasertpong, Y. Hikosaka, K. Nakamura, H. Saito, M. Takenaka, and S. Takagi, "Strategy toward HZO BEOL-FeRAM with low-voltage operation ($\leq$1.2 V), low process temperature, and high endurance by thickness scaling," in *Proc. Symp. VLSI Technol.*, vol. 17, Jun. 2021, pp. 1–2.

[8] Y.-K. Liang, J.-S. Wu, C.-Y. Teng, H.-L. Ko, Q.-H. Luc, C.-J. Su, E.-Y. Chang, and C.-H. Lin, "Demonstration of highly robust 5 nm $Hf_{0.5}Zr_{0.5}O_2$ ultra-thin ferroelectric capacitor by improving interface quality," *IEEE Electron Device Lett.*, vol. 42, no. 9, pp. 1299–1302, Sep. 2021, doi: 10.1109/LED.2021.3102604.

[9] H. Kim, K. S. Dae, Y. Oh, S. Lee, Y. Lee, S. Ahn, J. H. Jang, and J. Ahn, "A simple strategy to realize super stable ferroelectric capacitor via interface engineering," *Adv. Mater. Inter.*, vol. 9, no. 15, May 2022, Art. no. 2102528, doi: 10.1002/admi.202102528.

[10] P. J. Liao, Y. K. Chang, Y.-H. Lee, Y. M. Lin, S. H. Yeong, R. L. Hwang, V. Hou, C. H. Nien, R. Lu, and C. T. Lin, "Characterization of fatigue and its recovery behavior in ferroelectric HfZrO," in *Proc. Symp. VLSI Technol.*, vol. 6, Jun. 2021, pp. 1–2.

[11] R. Cao, Q. Liu, M. Liu, B. Song, D. Shang, Y. Yang, Q. Luo, S. Wu, Y. Li, Y. Wang, and H. Lv, "Improvement of endurance in HZO-based ferroelectric capacitor using Ru electrode," *IEEE Electron Device Lett.*, vol. 40, no. 11, pp. 1744–1747, Nov. 2019, doi: 10.1109/LED.2019.2944960.

[12] S.-C. Chang, N. Haratipour, S. Shivaraman, C. Neumann, S. Atanasov, J. Peck, N. Kabir, I.-C. Tung, H. Liu, B. Krist, A. Oni, S. Sung, B. Doyle, G. Allen, C. Engel, A. Roy, T. Hoff, H. Li, F. Hamzaoglu, R. Bristol, M. Radosavljevic, B. Turkot, M. Metz, I. Young, J. Kavalieros, and U. Avci, "FeRAM using anti-ferroelectric capacitors for high-speed and high-density embedded memory," in *IEDM Tech. Dig.*, Dec. 2021, p. 33, doi: 10.1109/IEDM19574.2021.9720510.

[13] Y.-D. Lin, P.-C. Yeh, Y.-T. Tang, J.-W. Su, H.-Y. Yang, Y.-H. Chen, C.-P. Lin, P.-S. Yeh, J.-C. Chen, P.-J. Tzeng, M.-H. Lee, T.-H. Hou, S.-S. Sheu, W.-C. Lo, and C.-I. Wu, "Improving edge dead domain and endurance in scaled $HfZrO_x$ FeRAM," in *IEDM Tech. Dig.*, Dec. 2021, pp. 6.4.1–6.4.4, doi: 10.1109/IEDM19574.2021.9720692.

[14] T. Francois, C. Pellissier, S. Slesazeck, V. Havel, C. Richter, A. Makosiej, B. Giraud, E. T. Breyer, M. Materano, P. Chiquet, M. Bocquet, L. Grenouillet, E. Nowak, U. Schroeder, F. Gaillard, J. Coignus, P. Blaise, C. Carabasse, N. Vaxelaire, T. Magis, F. Aussenac, and V. Loup, "Demonstration of BEOL-compatible ferroelectric $Hf_{0.5}Zr_{0.5}O_2$ scaled FeRAM co-integrated with 130 nm CMOS for embedded NVM applications," in *IEDM Tech. Dig.*, Dec. 2019, p. 15, doi: 10.1109/IEDM19573.2019.8993485.

[15] Y. Zheng, Y. Zheng, Z. Gao, J.-H. Yuan, Y. Cheng, Q. Zhong, T. Xin, Y. Wang, C. Liu, Y. Huang, R. Huang, X. Miao, K.-H. Xue, and H. Lyu, "Atomic-scale characterization of defects generation during fatigue in ferroelectric $Hf_{0.5}Zr_{0.5}O_2$ films: Vacancy generation and lattice dislocation," in *IEDM Tech. Dig.*, Dec. 2021, p. 33, doi: 10.1109/IEDM19574.2021.9720565.

[16] T. Gong, L. Tao, J. Li, Y. Cheng, Y. Xu, W. Wei, P. Jiang, P. Yuan, Y. Wang, Y. Chen, Y. Ding, Y. Yang, Y. Wang, B. Chen, Q. Luo, S. S. Chung, S. Du, and M. Liu, "$10^5\times$ endurance improvement of FE-HZO by an innovative rejuvenation method for 1z node NV-DRAM applications," in *Proc. Symp. VLSI Technol.*, vol. 16, Jun. 2021, pp. 1–2.

[17] S. Nittayakasetwat and K. Kita, "Anomalous structural distortion—A possible origin for the waking-up of the spontaneous polarization in ferroelectric HfO_2," *Jpn. J. Appl. Phys.*, vol. 60, no. 7, Jun. 2021, Art. no. 070908, doi: 10.35848/1347-4065/ac085c.

[18] M. Pešić, U. Schroeder, S. Slesazeck, and T. Mikolajick, "Comparative study of reliability of ferroelectric and anti-ferroelectric memories," *IEEE Trans. Device Mater. Rel.*, vol. 18, no. 2, pp. 154–162, Jun. 2018. doi: 10.1109/TDMR.2018.2829112.

[19] C. Lo, C.-K. Chen, C.-F. Chang, F.-S. Zhang, Z.-H. Lu, and T.-S. Chao, "High endurance and low fatigue effect of bilayer stacked anti-ferroelectric/ferroelectric $Hf_xZr_{1-x}O_2$," *IEEE Electron Device Lett.*, vol. 43, no. 2, pp. 224–227, Feb. 2022, doi: 10.1109/LED.2021.3134178.

[20] Z. Liang, K. Tang, J. Dong, Q. Li, Y. Zhou, R. Zhu, Y. Wu, D. Han, and R. Huang, "A novel high-endurance FeFET memory device based on ZrO_2 anti-ferroelectric and IGZO channel," in *IEDM Tech. Dig.*, Dec. 2021, p. 17, doi: 10.1109/IEDM19574.2021.9720627.

[21] M. Pešić, M. Hoffmann, C. Richter, T. Mikolajick, and U. Schroeder, "Nonvolatile random access memory and energy storage based on antiferroelectric like hysteresis in ZrO_2," *Adv. Funct. Mater.*, vol. 26, no. 41, pp. 7486–7494, Nov. 2016, doi: 10.1002/adfm.201603182.

[22] T. Onaya, T. Nabatame, M. Inoue, Y. C. Jung, H. Hernandez-Arriaga, J. Mohan, H. S. Kim, N. Sawamoto, T. Nagata, and J. Kim, "Improvement of ferroelectricity and fatigue property of thicker $Hf_xZr_{1-x}O_2/ZrO_2$ bi-layer," *ECS Trans.*, vol. 98, no. 3, pp. 63–70, Sep. 2020, doi: 10.1149/09803.0063ecst.

[23] M. H. Park, Y. H. Lee, H. J. Kim, Y. J. Kim, T. Moon, K. D. Kim, J. Müller, A. Kersch, U. Schroeder, T. Mikolajick, and C. S. Hwang, "Ferroelectricity and antiferroelectricity of doped thin HfO_2-based films," *Adv. Mater.*, vol. 27, no. 11, pp. 1811–1831, Mar. 2015, doi: 10.1002/adma.201404531.

[24] S. E. Reyes-Lillo, K. F. Garrity, and K. M. Rabe, "Antiferroelectricity in thin-film ZrO_2 from first principles," *Phys. Rev. B, Condens. Matter*, vol. 90, Oct. 2014, Art. no. 140103, doi: 10.1103/PhysRevB.90.140103.

[25] Y. Xu, Y. Yang, S. Zhao, T. Gong, P. Jiang, Y. Wang, P. Yuan, Z. Dang, Y. Chen, S. Lv, Y. Ding, Y. Wang, J. Bi, and Q. Luo, "Improved multibit storage reliability by design of ferroelectric modulated antiferroelectric memory," *IEEE Trans. Electron Devices*, vol. 69, no. 4, pp. 2145–2150, Apr. 2022, doi: 10.1109/TED.2021.3139054.

[26] V. M. Fridkin and S. Ducharme, "General features of the intrinsic ferroelectric coercive field," *Phys. Solid State*, vol. 43, no. 7, pp. 1320–1324, Jul. 2001, doi: 10.1134/1.1386472.

[27] E. K. Akdogan and A. Safari, "Size effects in nanophase $PbTiO_3$," in *Proc. IEEE Int. Symp. Appl. Ferroelectr.*, vol. 1, Jul. 2000, pp. 487–490, doi: 10.1109/ISAF.2000.941603.

[28] M. D. Glinchuk, A. N. Morozovska, A. Lukowiak, W. Strek, M. V. Silibin, D. V. Karpinsky, Y. Kim, and S. V. Kalinin, "Possible electrochemical origin of ferroelectricity in HfO_2 thin films," *J. Alloys Compounds*, vol. 830, Jul. 2020, Art. no. 153628, doi: 10.1016/j.jallcom.2019.153628.

[29] T. Schenk, E. Yurchuk, S. Mueller, U. Schroeder, S. Starschich, U. Böttger, and T. Mikolajick, "About the deformation of ferroelectric hystereses," *Appl. Phys. Rev.*, vol. 1, no. 4, Dec. 2014, Art. no. 041103, doi: 10.1063/1.4902396.